JOURNAL OF MATERIALS SCIENCE **40** (2005) 5627–5633

Dissolution behaviour of plasma sprayed apatite coatings

S. E. ETOK, K. D. ROGERS
Department of Materials & Medical Sciences, Cranfield University, Shrivenham, Swindon, Wiltshire SN6 8LA, UK
E-mail: k.d.rogers@cranfield.ac.uk

R. SCOTT
Biomet-Europe Ltd., Dorcan, Swindon, Wiltshire SN3 5HY, UK

Published online: 25 August 2005

Understanding the interaction of bioactive coatings with aqueous media is essential for development of systems possessing rapid osteointegration and durability. An *in vitro* study of a commercial, plasma sprayed hydroxyapatite coating has been undertaken. The coating behaviour when test coupons were immersed in water, simulated body fluid and foetal calf serum has been examined. The principal aim was to characterise, in detail, any structural changes to the coatings and, in particular, examine features of any new layers formed.

The amorphous phase of the coating showed preferential dissolution in all media. The rate of dissolution was greatest in water and the process was initially retarded in the foetal calf serum. A nanocrystallite apatite layer was shown to precipitate on the coatings in all media although this was significantly enhanced in simulated body fluid. The features of this layer (e.g., lattice parameters, crystallite size etc.) were quantified by adopting a novel approach to the X-ray diffraction data analysis.

The results are discussed in the context of similar studies and implications for *in vivo* behaviour.

1. Introduction

The use of bioactive material as a substitute for natural bone is an attractive proposition. Direct replacement by calcium hydroxyapatite however, is not generally possible in load bearing positions due to its brittleness and low tensile strength [1]. Coating metal orthopaedic endoprostheses with apatitic bioactive coatings to promote fixation and osteointegration is becoming increasingly common practice and more routes to coating fabrication are being developed. Calcium hydroxyapatite (HAP) is a particularly attractive coating material as it induces physiochemical bonding at HAP-bone interfaces and promotes bone growth with relatively high growing in rates.

Plasma spraying is used to produce almost all commercially available HAP coatings for orthopaedic and dental implants. Coatings are built up from partially melted powder particles, and are thus a heterogeneous mix of unmelted crystallites of the original powder, surrounded by amorphous calcium phosphate (ACP). Often, additional crystalline phases, such as CaO, are also found within the coatings [2]. The amorphous material and other phases are significantly more soluble than hydroxyapatite, and hence these are preferentially dissolved *in vitro* [3]. This leads to fragmentation of the coating, which, *in vivo* can result in the release of particles into surrounding tissues. Porosity can accelerate this process and the particles can potentially contribute to cell-mediated osteolysis. However, some degree of dissolution is an essential part of the mechanism by which biological fixation occurs, although if dissolution is too rapid, this can lead to the loss of mechanical fixation before the implant can be stabilised by bone attachment and ingrowth.

There have been several previous studies of the *in vitro* dissolution processes associated with plasma sprayed coatings [4, 5]. Generally, the dissolution mechanisms are characterised through measurement of the chemical changes to the physiological media into which coatings are immersed. Frequently, simulated body fluid (SBF) is employed as the media to model *in vivo* bioactivity although, of course, this does not provide information concerning protein interaction effects.

Recently, the formation of nanocrystalline apatite layers upon crystalline HAP by immersion in SBF has been studied by X-ray diffraction (XRD) and X-ray photoelectron spectroscopy [6]. A mechanism for the dissolution and subsequent precipitation of carbonated apatite was proposed based upon ion exchange between

0022-2461
DOI: 10.1007/s10853-005-1425-x

the SBF and HAP. However, this work presented several curiosities including (i) a decrease in estimated HAP crystallite size with increasing immersion time, (ii) a poor fit of the scattering associated with the (002) Bragg maxima between experimental data and that calculated from a structural model and, (iii) lattice parameter changes that were interpreted as an ion exchange mechanism more commonly associated with apatites produced at high temperatures.

In contrast to previous studies [7–10], which investigated only the relationship between coating characteristics and dissolution, the principal aim of this study was to highlight the microstructural (in terms of crystallite sizes and microstrain) and chemical changes (and hence bioactivity) occurring in these commercial coatings. It has been proposed previously [11], that structural and chemical properties of coatings will change after different degrees of dissolution, which will ultimately affect clinical performance. The work presented here is a detailed study of the apatite layer formed when a commercial prosthetic coating is immersed for increasing time periods in water, SBF and foetal calf serum (FCS). We have adopted a new approach to the diffraction analysis that has enabled further understanding of the dissolution-precipitation process.

2. Methods and materials

2.1. Growth

Initially, coatings were formed by plasma spraying an HAP stock powder onto titanium substrate disks (diameter ∼2 cm). In brief, the plasma spraying was achieved with a Plasma-Technic Type F4-MB plasma gun using argon as the primary gas. The resultant, uniform coatings were typically 50–80 μm thick. Within the X-ray interaction volume, the coatings were determined to consist of crystalline hydroxyapatite (∼60 wt%, HAP) and an amorphous calcium phosphate phase. There were no extraneous phases identified. These test samples were then washed in deionised water and immersed in various media for a range of times. The 3 media were deionised water, simulated body fluid [12] and foetal calf serum. A pair of samples was placed in 100 ml of each media and kept within an incubator at 37°C. Media without the presence of test disks served as controls. Each sample was characterised (see below) prior to immersion. After 1, 3, 7, 14 and 21 days under static conditions (i.e., not stirred) each sample was removed, washed in distilled water, dried in air and re-characterised. The media was also replenished and stored pending analysis at each of the characterisation times [13]. Dynamic conditions were not considered here.

2.2. Characterisation

The samples were visually inspected for indications of delamination and contamination and then weighed prior to further analysis. Analysis of the coated samples was carried out *in situ* by conventional powder X-ray diffractometry. Diffraction data was collected using a Philips PW1830 diffractometer fitted with a diffracted beam monochromator to produce diffractograms from Cu Kα wavelengths. Data was collected in the range 10° to 100°/2θ. Phase identification was performed with reference to the database supplied by the International Centre for Diffraction Data using the software, 'CSM' (Oxford Cryosystems).

A relatively new, 'standardless' method was applied to the diffractograms and this provided quantitative phase estimation (including the amorphous phase) and microstructural analysis. This methodology was essential as the coatings could be examined *in situ*; it would have been impossible to follow the conventional technique of 'spiking' the samples to determine the amorphous content. This approach, based upon whole pattern fitting (Rietveld analysis) [14] had been previously validated and theoretically justified for glass-ceramic mixes [15] and plasma sprayed hydroxyapatite coatings [16]. In essence, the fitting procedures adopted were the same as those for conventional Rietveld analysis although the structural models were fixed throughout. The process is described below in more detail.

Our model refinements were undertaken using TOPAS (Bruker–XAS) with fixed atomic structural parameter values acquired from the Inorganic Crystal Structural Database [17]. An influential parameter in this analysis for accurate quantification was appropriate choice of background. The background shape was determined empirically using data from substrates with their coatings removed and this was represented by a 1st order Chebychev polynomial.

In all refinements, the scale factors (enabling determination of relative wt%), lattice parameters, and peak shapes were refined for all crystalline phases. An advantage of this approach is that preferred orientation could also be included and accounted for (in this case using spherical harmonics) in the fitting process. Further, in principle, the method is capable of refining phases that possess very similar crystallographic features. In practice this required high quality data to reduce correlations between variables.

X-ray diffraction studies were complimented by Fourier transform infrared spectroscopy (VECTOR FT-IR/NIR Spectrometer with OPUS 3.1 software) mesaurements. The HAP coatings were analysed in the 4000–400 cm^{-1} region, at day 0, 7 and 14 of immersion. The KBr support discs used for the analysis were prepared with powder scrapped from the coating.

Ionic concentrations of calcium and phosphate present in the media and controls were measured before and after the period of immersion. Calcium ion concentration was measured by atomic absorption spectrophotometer (AAS). The instrument was calibrated with five point calibration using standards at 1, 2, 3, 4 and 5 μg/ml respectively. Strontium chloride was added to the media, controls and standards at this point because the measurement of calcium is disturbed by the presence of other metal ions. Phosphate ion concentration was measured using a Dionex DX-100 ion chromatography system calibrated with four point

calibration using standards at 20, 40, 60 and 80 μg/ml of phosphate respectively.

An environmental scanning electron microscopy (ESEM - LEO 435VP) was used to observe the changes in coating surface morphology before and after each immersion period. This system enables high quality images to be produced without the need for application of a conductive surface layer. Hence the same sample would be used for subsequent dissolutions.

3. Results

The pair of test samples within each media were independently analysed and no significant differences in behaviour could be determined. However, when comparing the samples from each media, significant differences in modifications to the coating structure were observed.

Fig. 1 shows diffractograms for a sample immersed in SBF at each measurement period. The data have been truncated in 2θ and offset in intensity, for clarity. As with all the samples, the data measured prior to immersion indicated a mix of crystalline and amorphous (seen most clearly as a background 'halo' between ~25–35°/2θ) material. No Bragg peaks from the titanium substrate were apparent as the 99% interrogation depth (~20 μm) of the X-rays was significantly less than the coating initial thickness. After 3 days immersion the amorphous halo had significantly reduced indicating loss of amorphous material. Careful inspection revealed that, after 7 days, there was a distinctive change in shape of the crystalline phase Bragg peaks. Each Bragg maxima appeared to develop extended 'tails' that increased in relative magnitude with increasing immersion time. Although not as pronounced, samples immersed in water also showed this feature. We have interpreted this as the formation of nanocrystalline apatite phase (nano-AP) and have been able to include this as an additional phase in the structural models required for whole diffraction pattern fitting. Some justification for this is shown in Fig. 2 where a substantially improved fit between observed and calculated data was obtained when the nanocrystalline material was included. Typically, the change in R_{wp} value when the nanocrystalline model was included (i.e. 2 lattice parameters, a scale factor and a crystallite size parameter) was from 13 to

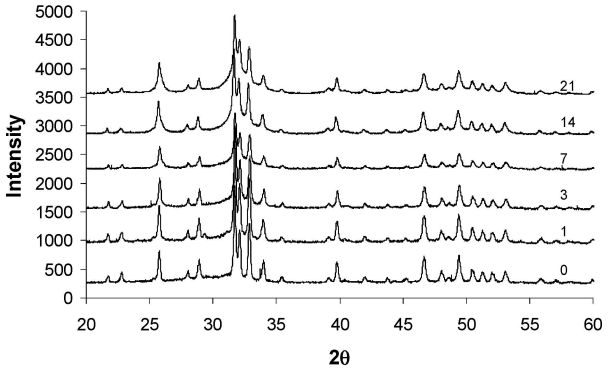

Figure 1 X-ray diffractograms from PS coatings immersed in SBF for an increasing number of days. All discrete maxima correspond to hydroxyapatite. Data are vertically offset for clarity

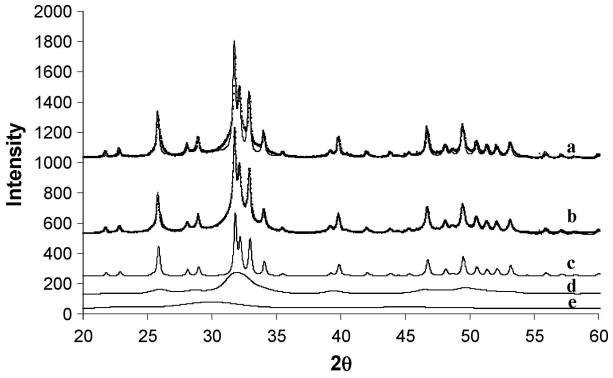

Figure 2 Calculated (—) and observed (•) diffraction data corresponding to a PS coating following immersion in SBF for 21 days. (a) is calculated from the sum of crystalline (c) and amorphous (e) components. The diffractogram in (b) is calculated from the sum of crystalline (c), amorphous (e) and nano-AP (d) components. Note the significantly improved fit when (d) is included within the structural model.

6% from the 21 day, SBF samples. The lattice parameters, crystallite size and scale factor of this phase were refined during each analysis. The results presented here are based upon the inclusion of all 3 phases at each immersion time.

Fig. 3 shows the changes to the weight proportions of the interrogated mass of the coating for ACP and nano-AP phase. Each data point is an average of that determined for each sample pair. The HAP and ACP scaling factors were corrected for absorption in the nano-AP using a thickness estimate from the mass measurements and assuming a uniform coating. Density was derived from the unit cell contents and refined lattice parameters of the nano-AP. Within water there was an immediate and relatively rapid fall in the wt% of the ACP compared to that of samples within SBF. There would appear to be no significant change in the ACP wt% of samples immersed in FCS. Fig. 3b indicates that coatings immersed in SBF contained a significantly greater proportion of nano-AP than the FCS and water samples. Both water and SBF samples showed small amounts of nano-AP after 1 day although no nano-AP could be detected on the samples within FCS. These compositional changes were also studied by examination of the diffraction data from the (002) Bragg peak i.e., at ~0.34 nm. A pair of analytical profiles (pseudo-Voigt) was independently fitted to the diffraction data to represent scattering from the HAP and nano-AP in this region. This excluded any contribution from the ACP and provided peak areas, positions and shapes from each phase. The area of each peak is presented in Fig. 4 and this shows an increase in peak area of the nano-AP and decrease in area of the HAP with increasing immersion time in SBF. Up to 3 days the data is perhaps unreliable due to high interphase correlations in the fitting process, (hence demonstrating a strength of whole pattern fitting). The data is not significantly influenced by preferred orientation as the whole pattern fitting indicated no change to this with media or immersion time. Thus, the increase in nano-AP peak area may be attributable to increasing phase absolute mass and the decrease in HAP peak area may be attributable to both a decrease in HAP mass and

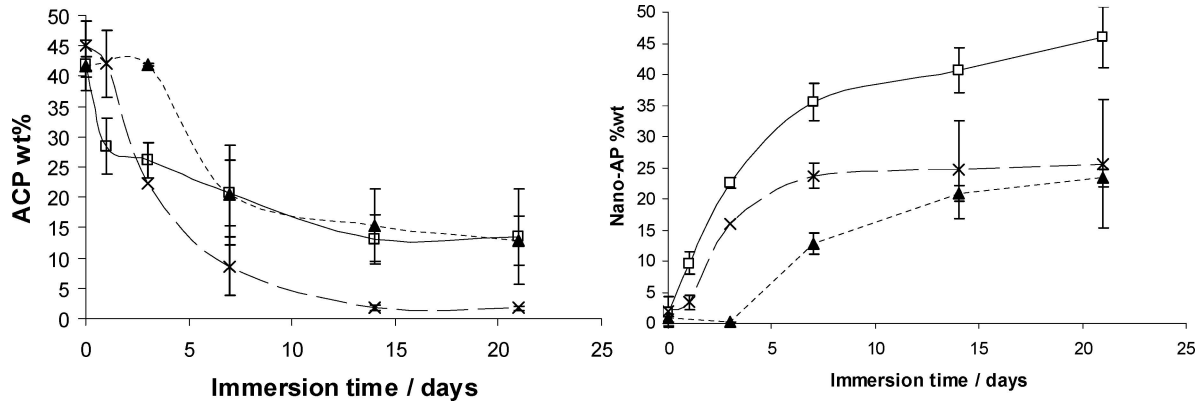

Figure 3 Calculated wt% of ACP (a) and nano-AP (b) within PS coatings for increasing immersion times in SBF (□), water (X) and FCS (▲). Error bars are standard deviations from the fitting process.

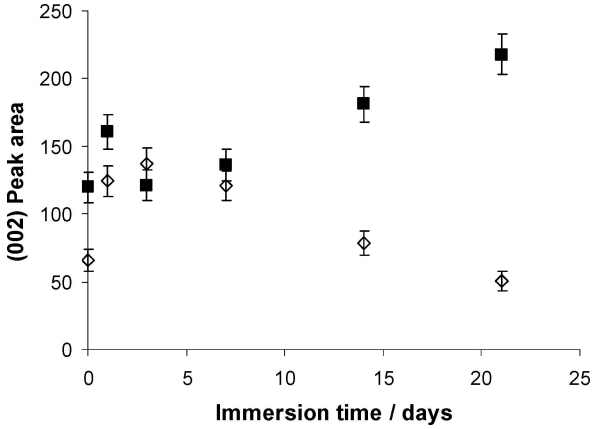

Figure 4 The change is hydroxyapatite, (002) Bragg peak area for coatings immersed for increasing times in SBF. (◇) – HAP, (■) – nano-AP. The error bars correspond to the standard deviations of measurements from different samples at each time point.

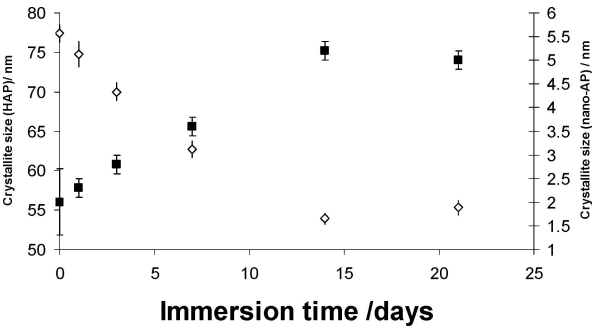

Figure 5 Crystallite size of the HAP (◇) and nano-AP (■) when samples were immersed in SBF for an increasing time. Error bars are derived from the fitting process

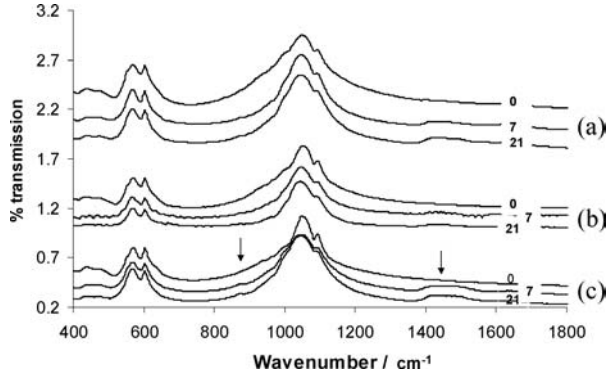

Figure 6 FTIR spectrograms of samples immersed ibn (a) FCS, (b) water and (c) SFB for 0, 7 and 21 days. Bands corresponding to CO_3^{-2} are indicated.

increased absorption due to the formation of surface nano-AP. In order to characterise the growth process further, the crystallite size of the HAP and nano-AP, as determined from the (002) refinements, is shown in Fig. 5. This assumes that all the peak broadening was attributable to finite crystallite size effects (see Discussion) but does not provide any information concerning size distributions. There is a clear decrease in HAP crystallite size and an increase in nano-AP size.

An indication of changes to lattice chemistry was derived by inspection of the lattice parameters of the HAP and nano-AP. In general there were only slight changes to the lattice parameters of each phase with immersion time ('*a*' showed a small increase and '*c*' a small decrease) and no significant differences between each media. However, the lattice parameters of the nano-AP were significantly different to those of the HAP. For example, after 21 days in SBF, the lattice parameters of the HAP were, $a = 0.94157(6)$ nm, $c = 0.68896(5)$ nm whereas for the nano-AP, $a = 0.9501(4)$, $c = 0.6866(4)$. The numbers in parenthesis are the estimated standard deviations from the fitting process.

The chemical nature of the coating was also examined by FTIR. Absorbance spectra for samples within each media are presented in Fig. 6. Prior to immersion the sample spectra were typical of those for hydroxyapatite. The most significant changes upon immersion are the appearance of absorption bands at 970 cm^{-1} and 1400–1600 cm^{-1}. These can be seen most clearly in the data corresponding to immersion in SBF. There is also a small decrease in resolution of the bands at 500–700 cm^{-1} (this has been employed [18] as a 'splitting factor' to previously characterise apatites). These changes have occurred in the period up to day 7, with no significant changes to the spectra between days 7 and 14.

A sharp but weak hydroxyl stretch bond vibration is observed at approximately 3570 cm^{-1} in all as-received samples. With increasing immersion time in SBF, the peak decreases and eventually disappears by day 14. This suggests that there is a decrease in number of

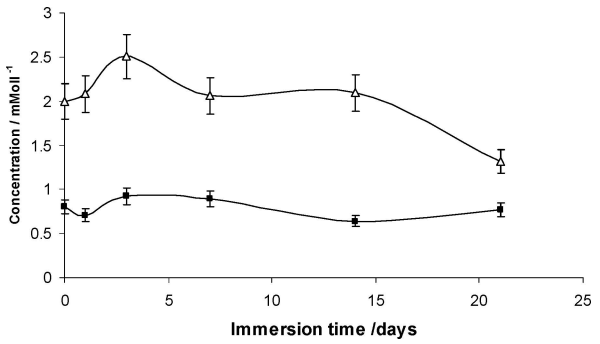

Figure 7 Changes in calcium (△) and phosphate (■) concentration of SBF for increasing time periods.

hydroxyl ions in the samples. In contrast, the hydroxyl stretch bond vibration is visible in the water samples, although it is reduced in comparison to the as-received samples.

No peaks corresponding to carbonate were detected in the water samples until day 14. In contrast, in the SBF samples, the appearance of CO_3 vibrational bands at approximately 1427, 1450 and 870 cm^{-1} was observed after the first week of immersion. This indicates that carbonate-substituted calcium phosphate had been precipitated during immersion. This is consistent with results obtained by previously [19].

The phosphate and calcium ion concentrations within the SBF determined at each inspection time, are presented in Fig. 7. The concentration of calcium and phosphate ions present in the media increased with immersion time and reached a maximum between day 1 and day 3. This period of corresponds with the period of rapid dissolution of ACP (Fig. 3), when free calcium and phosphate ions are liberated into solution. A significant decrease in calcium concentration is then observed between day 3 and day 21 which corresponds with the period where precipitation dominates. In contrast, the media retrieved from samples immersed in FCS showed no significant change in calcium or phosphate content which suggests that little dissolution had occurred.

ESEM analysis revealed that the as-received coatings had the morphology typical of plasma-sprayed coatings (Fig. 8a). This consisted of a lamellar microstructure composed of well-flattened splats and spherical droplets with tiny pores and micro-cracks [20, 21]. After the first day of immersion in SBF, it was apparent that the spherical droplets and flattened splats on the surface of the coatings had undergone some dissolution. The surfaces of the coatings showed signs of increased roughness and micro-crack propagation. At higher magnification (Fig. 8b), it was observed that the coating was covered in a newly formed layer of small granular structures. This dune-like film was characterized by numerous cracks of tortoiseshell character, which spread along the whole surface of the ceramic coating. As the immersion duration increased, the dune-like layer became denser and the granules in the layer became larger and hence more apparent, even at lower magnification, by day 7, (Fig. 8c). With a further increase in immersion time there was no significant change in morphology. By day 21, a dense, granular film was observed covering the surface of the ceramic coating (Fig. 8d). Other authors have reported the formation of needle-like crystal growth in dissolution studies [20, 22–25].

SEM analysis of the water samples revealed that, although more dissolution had occurred than in the SBF samples, significantly less newly formed precipitates appeared on the surface of the material (Fig. 9). A similar observation [23] as been previously explained using

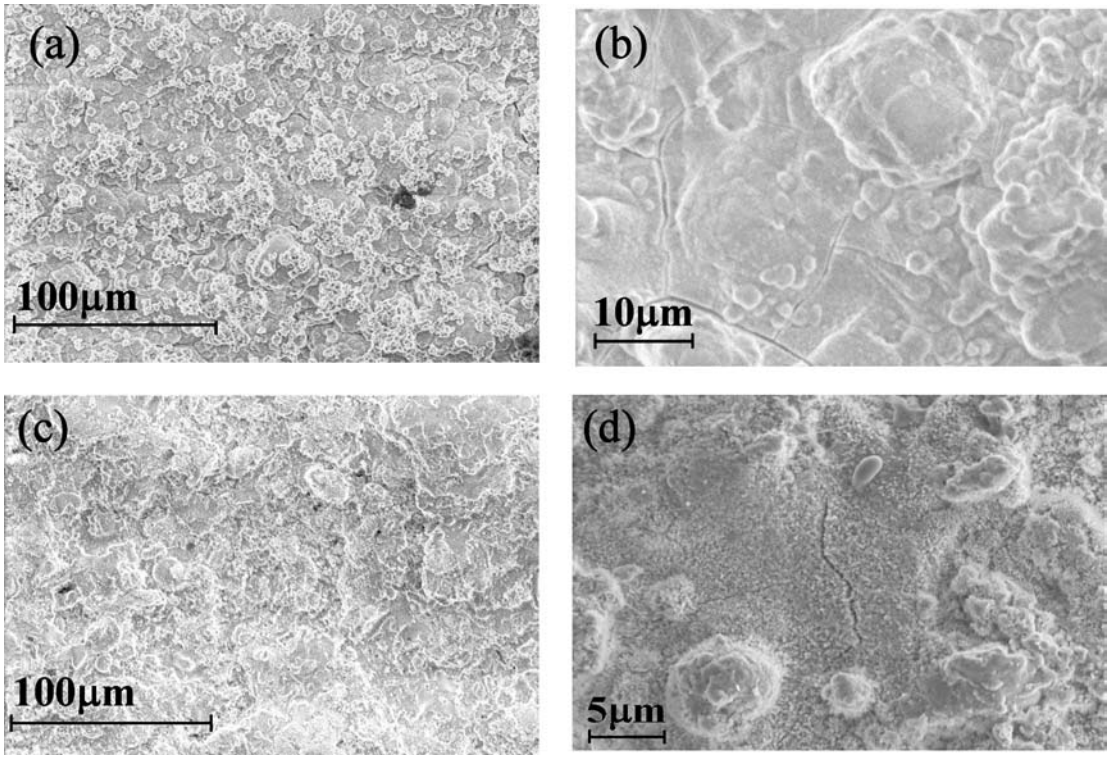

Figure 8 Electron micrographs of samples immersed in SBF for (a) 0 days, (b) 1 day (5000×), (c) 7 days (500×) and, (d) 21 days (7500×).

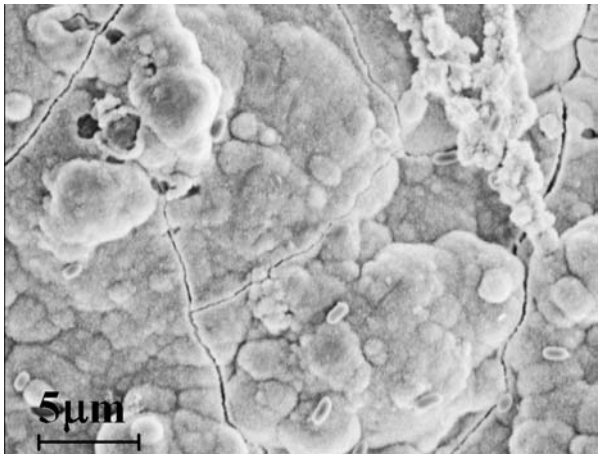

Figure 9 Electron micrograph of sample immersed in water at Day 21 (7500×).

classical nucleation theory. The nucleation and growth of an apatite layer, that is the result of the increased ion concentration by dissolution, will only occur when the favourable supersaturation is reached for heterogeneous nucleation or when the interfacial energy has been lowered [22].

4. Discussion

Overall, our results indicate the passive formation of an adherent, nanocrystalline hydroxyapatite phase from the dissolution and re-precipitation of the plasma sprayed coating material in water, SBF and FCS. It appeared that there is preferred dissolution of the amorphous phase of the materials. This has been quantified by the whole pattern fitting method employed here. The SBF solution contains calcium and phosphate ions and, once dissolution of the ceramic coatings commences, supersaturation is reached more rapidly than in the water which does not contain as high a concentration of free calcium and phosphate ions. It has been suggested previously [24] that, regardless of the crystalline phase, HAP will continue to dissolve as it is subjected to an under-saturated environment. This corroborates our observations that the samples immersed in water experienced a 33% loss in ACP compared to a 9% loss of ACP in the samples immersed in SBF over the 21-day immersion period.

The early stages of immersion are generally dominated by rapid dissolution of ACP and precipitation of nano-AP. In SBF the wt% of nano-AP appears to proceed through an initial rapid phase followed by a less rapid growth. As precipitation proceeds an increasing continuous apatite layer is formed that effectively inhibits further dissolution [25]. The plateau regions in Fig. 3 support this model. Crack propagation, increased porosity and surface roughness are generally the result of ion diffusion from the coating surface and the surrounding media. Previous authors [6, 20, 22, 26], have reported the same phenomenon in similar dissolution studies. It is likely that the surface roughness of the ceramic coatings provided nucleation sites for apatite precipitation. Although dissolution in water is more rapid than the other media, immersion in SBF forms an apatite layer of greater mass. Immersion in FCS would appear to impede dissolution (and thus subsequent layer formation).

Our estimates of crystallite size assume that there was negligible microstrain. This approximation is likely to be incorrect for HAP, as on consideration of the instrumental resolution function, the width of the Bragg peaks were found to have a dependence upon scattering angle. However, this was found not to be the case for peaks corresponding to the nano-AP. Thus it should be appreciated that, although the data is precise, its accuracy may be limited and also the values are an average of crystallographic directions through the nano-AP layer depth. The apparent increase in crystallite size (and/or reduction is strain) prior to day 14 creates an average domain size of approximately 5 nm. The Ostwald ripening shown to occur in nano-apatites from the dissolution of ACP [27] is not well demonstrated because ACP from the aqueous reaction system has not entirely disappeared and the nucleation of many small crystals reduces the degree of supersaturation.

The results of FTIR examination indicates inclusion of carbonate which we have estimated to be <2 wt%. It is suggested that this is present within the newly forming nano-AP. Surprisingly, this is not reflected in lattice parameter differences between HAP and nano-AP.

Similar dissolution studies have been carried out by previously [28], and although in this case the initial coatings were reported to consist of only crystalline HAP and traces of β-tricalcium phosphate (no ACP), the formation of a nano-AP phase was observed by SEM. It is probable that the poor fit between observed and calculated XRD data associated with the (002) Bragg maximum was also due to the nano-AP rather than preferred orientation as suggested (the (004) peak is a good fit). This previous study also demonstrated decreases in crystallite size and c-axis and a slight increase in a-axis lattice parameter with increasing immersion time. However, these findings are likely confounded as the nano-AP and crystalline component were not separated in the structural models used.

An ideal coating is one which exhibits slow, uniform resorbtion, at a rate which allows the bone to replace the reabsorbed coating. During this process, the coating should remain intact and attached to the implant. Ideally, therefore, the coating therefore should be dense, strongly bonded to the substrate, and macroscopically homogenous. This cannot be achieved by plasma spray, since by the nature of the process, the coatings are heterogeneous. High crystallinity coatings, which have only a small amount of amorphous material holding the particles together, thus exhibit poor cohesion and adhesion to the substrate, and a high level of porosity.

Despite the superficial understanding of the exact mechanisms involved, *in vivo* coating resorption can be categorised as two simultaneous processes; namely dissolution-precipitation at neutral pH (between bone and the coating through ionic species, Ca^{2+}, OH^{-}, PO_4^{3-}, carried by body fluid) and osteoclastic bone modelling [10, 29–31]. Nonetheless, dissolution-precipitation remains the key factor affecting

bioactivity, which is inherently affected by characteristics of both the HAP coatings and the physiological environment [32].

The results of this study emphasis that plasma sprayed coatings exhibit an ability to promote the formation of a carbonated nano-AP (bone-like apatite) layer. The formation of the carbonated layer appears to be accelerated by the presence of free calcium and phosphate ions in the media. No significant change in morphology of chemical nature of the coatings immersed in FCS was observed. These results are consistent with findings that the presence of blood proteins in the FCS have an inhibitory effect on the dissolution and hence HAP crystal nucleation and growth [29].

5. Conclusions

It has been demonstrated that this novel approach to X-ray diffraction analysis, enables the crystalline, semi-crystalline and amorphous components of commercial coatings to be modelled as independent phases. Changes in microstructural and chemical nature of the coatings with immersion time can thus be quantified. To evaluate the biological response of coatings, their *in vitro* behaviour was investigated following immersion in deionised water, SBF and FCS for a period of up to 21 days. Samples immersed in SBF and water were observed to undergo an initial rapid dissolution of ACP followed by a subsequent precipitation of carbonated nano-AP. Increased immersion time promoted nucleation and rapid growth of the carbonated nano-AP crystals on coatings immersed in both water and SBF. Despite significantly more dissolution occurring in the samples immersed in water, nano-AP formation was more extensive in the coatings immersed in SBF. Carbonated nano-AP precipitation may be thermodynamically and kinematically more favourable in SBF than in water [28].

References

1. R. MARTIN and *P. J. BROWN*, *J. Mat. Sci. Mat. Med.* **6**(3) (1995) 138.
2. K. A. GROSS and C. C. BERNDT, *J. Biomed. Mat. Res.* **39**(4) (1998) 580.
3. L. SUN, C. C. BERNDT, K. A. KHOR, H. N. CHEANG and K. A. GROSS, *ibid.* **62**(2) (1998) 228.
4. L. SUN, C. C. BERNDT, K. A. GROSS and A. KUCUK, *ibid.* **58**(5) (2001) 570.
5. J. WENG, Q. LIU, G. J. C. WOLKE, D. ZHANG and K. DEGROOT, *J. Mat. Sci. Lett.* **16**(4) (1997) 335.
6. Y. W. GU, N. H. LOH, K. A. KHOR, S. B. TOR and P. CHEANG, *Biomaterials* **24** (2003) 1603.
7. F. BARRERE, M. STIGTER, P. LAYROLLE, C. A. VAN BLITTERSWIJK and K. DE GROOT, *Key Engng. Mater* **192–195** (2001) 67.
8. L. C. CHOW, *J. Ceram. Soc, Japan* **99** (1991) 954.
9. S. R. LEADLEY, M. C. DAVIES, C. CASTRO RIBEIRO, M. A. BARBOSA, A. J. PAUL and J. F. WATTS, *Biomaterials* **18**(4) (1997) 311.
10. E. MAVROPOULOS, A. M. ROSSI, N. C. C. DA ROCHA, G. A. SOARES, J. C. MOREIRA and G. T. MOURE, *Mater. Char.* **50**(2–3) (2003) 203.
11. L. B. SUN, C. C. BERNDT, K. A. GROSS and A. KUCUK, in "Material Fundamentals and Clinical Performance of Plasma Sprayed Hydroxyapatite Coatings: A Review" (Centre for Thermal Spray Research, University of New York at Stony Brook, New York, 2001) p. 570.
12. T. KOKUBO, H. KUSHHITANI, S. KITSUGI and T. YAMAMURO, *J. Biomed. Mater. Res.* **24** (1990) 721.
13. S. E. ETOK and K. D. ROGERS, in "Bioceramics: Materials and Applications" V. edited by R. Rusin (American Ceramic Society. Indianapolis, USA, 2004).
14. H. RIETVELD, *J. Appl. Cryst.* **2** (1969) 65.
15. P. RIELLO, P. CANTON, N. COMELATO, S. POLIZZI, M. VERITA, G. FAGHERAZZI, H. HOFMEISTER and S. HOPFE, *J. Non-Cryst. Solids* **288**(1–3) (2001) 127.
16. K. D. ROGERS, S. E. ETOK and R. SCOTT, *J. Mater. Sci.* 2004 (in press).
17. D. A. FLETCHER, R. F. MCMEEKING and D. PARKIN, *J. Chem. Inf. Comut. Sci.* **36** (1996) 746.
18. D. LUCY and A. M. POLLARD, in Proccedings of the Conference on the Applications of Scientific Techniques to the Study of Archaeology (Oxbow Books, Liverpool, 1995).
19. A. C. QUEIROZ, J. D. SANTOS, F. J. MONTEIRO and M. H. PRADO DA SILVA, *Mater Char* **50**(2–3) (2003) 197.
20. J. WENG, Q. LUI, J. G. C. WOLKE, D. ZHANG and K. DE GROOT, *Mater. Sci. Lett.* **16** (1997) 335.
21. X. LIU, S. TAO and C. DING, *Biomaterials* **23** (2002) 963.
22. J. WENG, Q. LIU, J. G. C. WOLKE, X. ZHANG and K. DE GROOT, *ibid.* **18** (1997) 1027.
23. A. G. WALTON, "The Formation and Properties of Precipitates" (Interscience, New York, 1967).
24. E. P. PASCHALIS, Q. ZHAO, B. E. TUCKER, M. S, J. A. BEARCROFT, N. B. BEALS, M. SPECTOR and N. G. H, *J. Biomed. Mater. Res.* **29** (1995) 1499.
25. S. J. DING, C. P. JU and J. H. LIN, *J. Mater. Sci. Mater. Med.* **11** (2000) 183.
26. X. LIU, S. TAO and C. DING, *Biomaterials* **23** (2002) 963.
27. E. D. EANES and A. S. POSNER, *Mater. Res. Bull.* **5**(6) (1970) 377.
28. Y. W. GU, K. A. KHOR and P. CHEANG, *Biomaterials* **25** (2004) 4127.
29. V. SERGO, SBAIZERO and D. CLARKE, *ibid.* **18** (1997) 477.
30. L. SUN, C. C. BERNDT, K. A. KHOR, H. N. CHEANG and K. A. GROSS, *J. Biomed. Mater. Res.* **62** (2002) 228.
31. X. LU and Y. LENG, *Biomaterials* **26** (2005) 1097.
32. S. G. REES, D. T. HUGHES-WASSELL, R. P. SHELLIS and G. EMBREY, *Biomaterials* **25** (2004) 971.

Received 9 November 2004
and accepted 8 April 2005